Current Noise of Hydrodynamic Electrons

Aaron Hui and Brian Skinner
Department of Physics, Ohio State University, Columbus, Ohio 43202, USA

(Received 21 November 2022; accepted 4 May 2023; published 20 June 2023)

A resistor at finite temperature produces white noise fluctuations of the current called Johnson-Nyquist noise. Measuring the amplitude of this noise provides a powerful primary thermometry technique to access the electron temperature. In practical situations, however, one needs to generalize the Johnson-Nyquist theorem to handle spatially inhomogeneous temperature profiles. Recent work provided such a generalization for Ohmic devices obeying the Wiedemann-Franz law, but there is a need to provide a similar generalization for hydrodynamic electron systems, since hydrodynamic electrons provide unusual sensitivity for Johnson noise thermometry but they do not admit a local conductivity nor obey the Wiedemann-Franz law. Here we address this need by considering low-frequency Johnson noise in the hydrodynamic setting for a rectangular geometry. Unlike in the Ohmic setting, we find that the Johnson noise is geometry dependent due to nonlocal viscous gradients. Nonetheless, ignoring the geometric correction only leads to an error of at most 40% as compared to naively using the Ohmic result.

DOI: 10.1103/PhysRevLett.130.256301

Introduction.—The measurement of heat flow has long been a pivotal tool for exploring many-body systems in condensed matter and materials physics. For example, measurements of thermal conductivity or heat capacity reflect the existence of whichever quasiparticles are present in the system, including those which are charge neutral. But such measurements require an accurate thermometer, and modern metrology schemes increasingly require nanoscale temperature resolution.

In the context of electron systems, one challenge of nanoscale thermometry is to disentangle electron and phonon contributions to heat transport; in settings with weak electron-phonon coupling, the electron and phonon temperatures may not even be the same. Johnson noise thermometry addresses the electronic half of this issue: it is a powerful primary thermometry technique that allows one direct and isolated access to the electronic degrees of freedom. For this technique's simplest formulation, consider a resistor held at a uniform electronic temperature T_0. The Johnson-Nyquist theorem (fluctuation-dissipation theorem) dictates that in a two-terminal setup

$$S(t-t') \equiv \langle \delta I(t)\delta I(t')\rangle = \frac{2k_B T_0}{R}\delta(t-t'), \qquad (1)$$

where $\delta I(t) = I(t) - \langle I\rangle$ is the charge current fluctuation at time t and R is the resistance; $\langle \ldots \rangle$ denotes an ensemble average (i.e., a time average if ergodicity is assumed) [1]. As seen in Eq. (1), the time-averaged current fluctuations provide a direct measure of the temperature of the electron bath in the resistor. The noise correlator $S(t-t')$ can be written in units of temperature, defining the so-called Johnson noise temperature

$$T_{\mathrm{JN}} \equiv \lim_{\omega\to 0}\frac{R}{2k_B}S(\omega), \qquad (2)$$

where $S(\omega) = \int_{-\infty}^{\infty} dt\, e^{-i\omega t}S(t)$ is the (two-sided) Fourier transform of the current noise correlator. Therefore, in situations with uniform temperature the Johnson-Nyquist theorem tells us that $T_{\mathrm{JN}} = T_0$; the Johnson noise temperature directly measures the electronic temperature T_0 without need for calibration. In other words, Johnson noise acts as a primary thermometer. This thermometry technique has recently been fruitfully utilized to make record-sensitive bolometers [2–6] and to make measurements of electronic thermal conductivity and heat capacity [7–9].

In many practical situations, such as those listed above, the fundamental Eq. (1) does not apply since the electronic temperature is not spatially uniform. Generalizations of Eq. (1) were previously studied [10,11] for electronic systems that obey Ohm's law, i.e., where a local proportionality $J(\mathbf{x}) = \sigma(\mathbf{x})E(\mathbf{x})$ between current density and electric field holds, as well as the Wiedemann-Franz (WF) law. These studies find that when current flows through a two-terminal device, Joule heating leads to an increase in the measured Johnson noise (in temperature units) by

$$\delta T_{\mathrm{JN}} \equiv T_{\mathrm{JN}} - T_0 = \frac{PR}{12L_0T_0}. \qquad (3)$$

Here $P = I^2R$ is the Joule power, R is the resistance, and $L_0 = \kappa/(\sigma T_0) = (\pi^2/3)(k_B/e)^2$ is the Lorenz ratio. The quantity δT_{JN} can be thought of as the excess noise arising from Joule heating; throughout this Letter we refer to the total T_{JN} as simply the "Johnson noise." Equation (3) has been known for the special case of a rectangular geometry

with a spatially uniform and diagonal conductivity tensor since at least 1992 [12], but in fact Eq. (3) is generic for any two-terminal geometry and any form of the conductivity tensor (even if it exhibits spatial variations), so long as Ohm's law and the WF law are obeyed [11].

What has remained unknown is how Eq. (3) should be generalized for situations not governed by Ohm's law. Electronic systems that violate Ohm's law have become increasingly prominent in recent years, with experimental works demonstrating a hydrodynamic regime of strongly interacting electrons in a number of materials [13–40]. In such systems there is no concept of a spatially local conductivity and WF is violated. Graphene in particular is a material of choice both for Johnson noise thermometry and electron hydrodynamics, due to its relatively weak electron-phonon coupling, low disorder, and strong electron-electron interactions. The advent of these hydrodynamic electron systems calls for an extension of Johnson noise theory to this new setting.

Moreover, a naïve application of Eq. (3) (as was used, for example, in the seminal measurements of WF violation in graphene [20]) suggests great practical utility of hydrodynamic electrons. Electrons in the hydrodynamic regime can display large WF violations [20,34,41–50], and deep in the hydrodynamic regime (with only a single type of carrier) the Lorenz ratio $\kappa/(\sigma T_0)$ becomes very small [41–43,45,49]. Naively inserting this small effective Lorentz ratio into Eq. (3) suggests a very large sensitivity for Johnson noise in the hydrodynamic regime. Such high sensitivity would imply that hydrodynamic electrons are ideal for bolometry and thermometry applications. Therefore, the key question of the fate of thermal noise in a hydrodynamic electron system and the validity of Eq. (3) has significant practical and theoretical importance for the development of electron thermometry.

In this Letter, we explicitly study the Johnson noise of hydrodynamic electrons. We analytically solve for the low-frequency fluctuations of the Navier-Stokes equations in a rectangular geometry, depicted in Fig. 1. We find that the Johnson noise temperature is no longer geometry independent due to nonlocal viscous gradients, as opposed to the Ohmic case [11]. Despite this nonuniversality, Eq. (3) is of

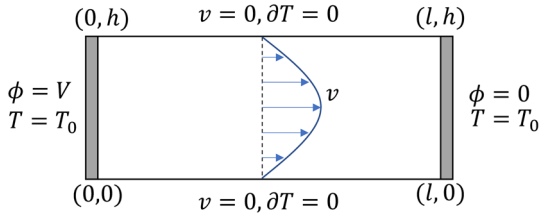

FIG. 1. The rectangular geometry that we consider and its boundary conditions. A voltage V is applied across the contacts, and we consider no-slip boundary conditions at the walls. We also fix the temperature on the x boundaries and enforce $\partial_y T = 0$ on the y boundaries.

the correct functional form up to a multiplicative geometric correction. In fact, this geometric correction is no larger than 40% for any aspect ratio of the system or any value of the electron-electron scattering rate. Thus, Eq. (3) provides a generally correct description of the Johnson noise, even though the resistance R and Lorenz ratio L are strongly renormalized by hydrodynamic effects.

Mathematical setup.—Throughout this Letter, we work with the rectangular geometry shown in Fig. 1. The full equations of motion for incompressible flow are given by

$$\partial_t \mathbf{v} + \mathbf{v}\cdot\nabla\mathbf{v} = -\frac{1}{\rho}\nabla P - \frac{q}{m}\nabla\phi - \gamma\mathbf{v} + \nu\nabla^2\mathbf{v}, \quad (4)$$

$$\partial_t T + \mathbf{v}\cdot\nabla T = \frac{\kappa}{2c_p}\nabla^2 T + \frac{\nu}{2c_p}(\partial_k v^i + \partial_i v^k)^2 + \frac{\gamma}{c_p}v^2, \quad (5)$$

$$\nabla\cdot\mathbf{v} = 0. \quad (6)$$

The hydrodynamic fields are the velocity v, the temperature T, the pressure P, and the electric potential ϕ. The phenomenological constants in the equations of motion are the hydrodynamic mass m, the charge q, the mass density ρ, the momentum relaxation rate γ, the viscosity ν, the specific heat at constant pressure c_p, and the thermal conductivity κ. We have assumed an incompressible flow with constant density [51]; this assumption is valid for flows with $v \ll c$ and $\tau \gg L/c$ where c is the speed of sound and τ and L are a characteristic time and length, respectively [52,53]. We also neglect the pressure P since it can be subsumed into an effective electric potential $\phi' = \phi + mP/(\rho q)$. Finally, we will work at linear order, neglecting convection terms $\mathbf{v}\cdot\nabla\mathbf{v}$ and thermal advection $\mathbf{v}\cdot\nabla T$. Dropping convection is valid at low Reynolds numbers $\mathrm{Re}_\nu \equiv vL/\nu \ll 1$ [54] or at low "momentum-relaxation Reynolds number" [55] $\mathrm{Re}_\gamma \equiv v/L\gamma \ll 1$. Graphene experiments are typically deep within this low Reynolds number regime, with $\gamma \sim 650$ GHz, $\nu \sim 0.1\,\mathrm{m}^2/\mathrm{s}$, and $L \sim 5$ μm [19] so that $\mathrm{Re}_\gamma \sim I/(26\ \mathrm{mA})$ and $\mathrm{Re}_\nu \sim I/(160\ \mu\mathrm{A})$ [55]. Moreover, dropping thermal advection is valid for $\kappa/(c_p L) \gg v$ when thermal diffusion is fast compared to the fluid velocity. After these simplifications, the equations of motion become

$$\partial_t \mathbf{v} = -\frac{q}{m}\nabla\phi - (\gamma - \nu\nabla^2)\mathbf{v}, \quad (7)$$

$$\partial_t T = \frac{\kappa}{2c_p}\nabla^2 T + \frac{\nu}{2c_p}(\partial_k v^i + \partial_i v^k)^2 + \frac{\gamma}{c_p}v^2, \quad (8)$$

$$\nabla\cdot\mathbf{v} = 0. \quad (9)$$

Equation (7) is the momentum balance equation with an electric force, momentum relaxation, and viscous drag. Equation (8) is the heat equation, with source terms from

viscous heating and Joule heating. Supplemented by fixed-voltage, fixed-temperature, and no-slip or no-heat-flow boundary conditions (see Fig. 1), solving these equations provides the quasi-equilibrium solution about which we will study noise fluctuations.

Once the steady-state solution is known, we can study the thermal noise fluctuations. We are interested in low frequency solutions, $s \to 0$, where the velocity fluctuations δv_i are described by the Laplace transform of Eq. (7) [56]

$$(s+\gamma-\nu\nabla_{\mathbf{r}}^2)\langle\delta v_i(\mathbf{r},s)\delta v_j(\mathbf{r}',0)\rangle = \langle\delta v_i(\mathbf{r},0)\delta v_j(\mathbf{r}',0)\rangle \equiv \frac{k_B T(\mathbf{r})}{\rho}\delta(\mathbf{r}-\mathbf{r}')\delta_{ij}, \tag{10}$$

where s is the Laplace parameter [57] and the initial condition on the rhs of Eq. (10) is given by the equipartition theorem. This equation is supplemented by incompressibility of fluctuations $\partial_i\langle\delta v_i(\mathbf{r},s)\delta v_j(\mathbf{r}',0)\rangle = 0$. In writing Eq. (10) with incompressibility, we have neglected the electric potential (pressure) and density fluctuations. This approximation is again valid when $\omega \ll c/L$, i.e., when the frequency is much smaller than the characteristic sound frequency of the sample. Finally, to obtain the current fluctuations from the velocity fluctuations, it is convenient to apply the relation $I = (1/\ell)\int dxdyJ_x$ to the solution of Eq. (10); this relation arises from current conservation since $\int dyJ_x$ is independent of x.

For simplicity, we ignore other forms of noise that may be present. Shot noise, in particular, is also present; for diffusive conductors it dominates whenever the source-drain voltage V is large enough that $eV \gg k_B T$ (see, e.g., Refs. [58,59]). However, recent experiments measuring Johnson noise in hydrodynamic electrons tend to operate in a regime where Johnson noise is dominant over shot noise [7–9,20,60]. We leave an exploration of other noise mechanisms in the hydrodynamic regime to future work.

Solution.—We begin by solving the steady-state equations of motion to determine the temperature profile. The steady-state velocity profile is given by the Ohmic-Poiseuille solution (see, e.g., Ref. [17])

$$J_x(y) \equiv n v_x(y) = \sigma_D E_x\left[1-\frac{\cosh(\frac{y-h/2}{\lambda})}{\cosh(\frac{h}{2\lambda})}\right], \tag{11}$$

where $\sigma_D \equiv ne^2/(m\gamma)$ is the Drude conductivity and the electric field $E_x = V/\ell$. The viscous length scale or Gurzhi length $\lambda \equiv \sqrt{\nu/\gamma}$ is a length scale below which viscous effects are important. For convenience, we can define an effective conductivity $\bar{\sigma} \equiv (\ell/h)/R = [1-(2\lambda/h)\tanh(h/2\lambda)]\sigma_D$, where the two-terminal resistance $R = V/I$ was computed using Eq. (11). In the Ohmic limit $\lambda \ll h$, the effective conductivity $\bar{\sigma} \to \sigma_D$ reduces to the usual Drude conductivity. We emphasize that a local conductivity is *not* well defined in the presence of viscosity; the effective conductivity is useful as a measure of the heat dissipation, not of the local current-voltage relation. The solution for the velocity profile in Eq. (11) determines the dissipative heating terms in Eq. (8), which allows us to solve for the temperature profile.

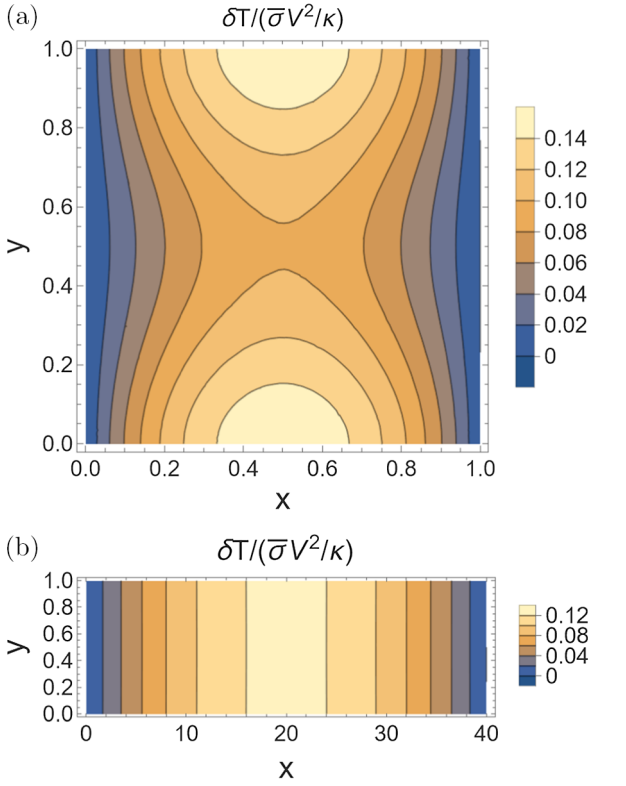

FIG. 2. A plot of the purely viscous ($\lambda \to \infty$) temperature profiles for (a) $h/\ell = 1$ and (b) $h/\ell = 1/40$. Notice that for (b), the profile is very similar to the Ohmic profile, having negligible y variation.

We use Fourier techniques to obtain the temperature profile analytically. The exact result can be written as

$$T(\mathbf{x}) = T_0 + \frac{\bar{\sigma}V^2}{\kappa}\left[\frac{1}{2}\tilde{x}(1-\tilde{x}) - \frac{h^2}{\ell^2}F\left(\frac{h}{\ell},\frac{\lambda}{h};\mathbf{x}\right)\right], \tag{12}$$

where $\tilde{x} = x/l$ is the nondimensionalized x coordinate and F is a double Fourier sum [61]. To obtain a qualitative understanding, we consider this result in various simplifying limits (see Fig. 2).

In the Ohmic limit $\lambda \ll h$, the heating profile (i.e., the heat per unit area generated at each point) is spatially uniform; since $F \to 0$, this limit admits the simple parabolic temperature profile

$$T_{\mathrm{Ohm}}(x) = T_0 + \frac{\bar{\sigma}V^2}{\kappa}\frac{1}{2}\tilde{x}(1-\tilde{x}) + \mathcal{O}(\lambda/h), \tag{13}$$

with $\bar{\sigma} \to \sigma_D$. This parabolic profile is the result of the thermal boundary conditions: heat is only allowed to flow at the contacts at $x = 0$ and $x = \ell$, so the temperature must be maximal in the center and minimal at the fixed-temperature boundaries.

In the opposite viscous limit, $\lambda \gg h$, viscous dissipation leads to a nonuniform heating along the y direction (though heating is still uniform in x, as in the Ohmic case). The temperature profile then obtains a "geometric correction" to the Ohmic result as a function of the aspect ratio h/ℓ. In the thin channel regime $h \ll \ell$, analyticity of F around $h/\ell = 0$ means that the temperature profile takes the simple form

$$T_{\text{thin}} = T_0 + \frac{\bar{\sigma} V^2}{\kappa} \frac{1}{2} \tilde{x}(1 - \tilde{x}) + \mathcal{O}(h^2/\ell^2). \tag{14}$$

This "Ohmic-like" temperature profile arises due to the fact that in the thin channel limit, the problem becomes quasi-1D; heating inhomogeneities rapidly equilibrate along y as compared to along x, leading to small, $\mathcal{O}(h^2/\ell^2)$ corrections to the Ohmic-like temperature profile that is independent of y. An example of an Ohmic-like temperature profile in the thin channel limit is plotted in Fig. 2(b).

As we will see below, the temperature profile determines the Johnson noise profile, so that correspondingly Eq. (3) is obeyed in both the Ohmic limit and the thin channel limit (for the latter, even in the limit of zero Drude resistivity, $\gamma \to 0$). Therefore, in order to observe any deviation from Eq. (3), one needs to be in the regime $\ell \gtrsim h \gtrsim \lambda$, for which the temperature profile is nonuniform in the y direction. An example is shown in Fig. 2(a), where one can see increased temperature at the boundaries due to viscous dissipation from the no-slip boundary friction.

Given the temperature profile, we can solve for the measured current noise via Eq. (10), again using Fourier techniques. The analytic result can be written as

$$S = \frac{2k_B}{R} \left[T_0 + \frac{\bar{\sigma} V^2}{12\kappa} f(h/\ell, \lambda/h) \right], \tag{15}$$

where the function f is a Fourier series and is plotted in Fig. 3 [61]. In the Ohmic limit $\lambda \ll h$, we find that $f \to 1$, recovering the previous Ohmic result for the Johnson noise [11] [see Eq. (3)].

$$S_{\text{Ohm}} = \frac{2k_B}{R} \left[T_0 + \frac{\sigma_D V^2}{12\kappa} \right]. \tag{16}$$

Therefore, we interpret f as a geometric correction to the Ohmic Johnson noise result. For $h \ll \ell$ where the temperature profile is Ohmic-like, we also obtain the Ohmic result $f \to 1$. Around $\lambda/h \sim 0.2$, we find that $f - 1$ changes sign. This sign change is due to a crossover from the regime where Joule heating dominates to the regime where viscous heating dominates, which produces a corresponding change

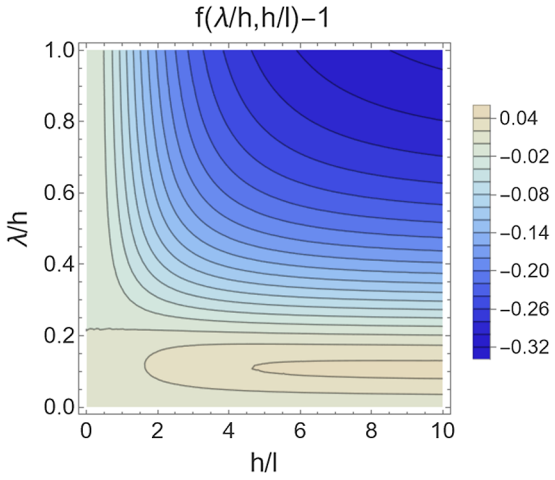

FIG. 3. A plot of $f(h/l, \lambda/h) - 1$, the deviation of the geometric correction to the Johnson noise from unity. In both the Ohmic limit, $\lambda/h \ll 1$, and the thin channel limit, $h/l \ll 1$, we find $f \to 1$. Viscous effects are most prominent for $\lambda/h \gg 1$ and $h/l \gg 1$, where $f \to 3/5$.

in the "topography" of the temperature profile. When Joule heating dominates ($\lambda/h \lesssim 0.2$) there is a single temperature peak in the center, while when viscous heating dominates ($\lambda/h \gtrsim 0.2$) there are two temperature peaks, one at each boundary.

In general, the dimensionless function f is a slow $\mathcal{O}(1)$ function of h/ℓ and λ/h and f never deviates from unity by more than 40%. Deep in the limit of viscous flow and large aspect ratio ($\lambda/h \gg 1$ and $h/\ell \gg 1$), i.e., the top-right corner of Fig. 3, the value of f approaches $3/5$. Despite this conclusion that the Ohmic result of Eq. (3) is always "nearly correct," we emphasize that the sensitivity of Johnson noise thermometry is generally strongly renormalized by hydrodynamic effects. Specifically, viscous effects tend to strongly renormalize the resistance R and the Lorenz ratio $L = \kappa/(\bar{\sigma} T_0)$, thereby making a large quantitative change in the measured Johnson noise.

Conclusion.—In this Letter, we have shown that the relationship between Johnson noise and heating for Ohmic and WF-obeying systems [Eq. (3)] is, surprisingly, mostly valid even for hydrodynamic electrons [Eq. (10)]. A geometric correction arises from preferential heating near the no-slip boundaries by viscous shear, but this correction is never more than 40%, regardless of the sample's aspect ratio or viscosity. Our result enables a range of fundamental and applied applications in thermometry and bolometry, and justifies applying existing Johnson noise thermometry techniques (those of Refs. [8] and [9], for example) directly in the hydrodynamic regime.

Our results, derived for a Galilean-invariant fluid, can be directly extended to the "Dirac fluid" limit where n-type and p-type carriers coexist (as in graphene near the charge neutral point) [64]. In general, with chemical potential μ away from the Dirac point, electron-hole scattering causes

the majority carriers to drag the minority carriers, so that electrons and holes equilibrate to the same hydrodynamic drift velocity. Very near the Dirac point, however, there is a zero-momentum mode with disequilibrated electron and hole drift velocities that can also carry current. This zero-momentum mode can relax current via electron-hole scattering, increasing the current-relaxation rate and suppressing the viscous length λ. Therefore, when the chemical potential is sufficiently close to the Dirac point, the current noise should return to Ohmic-like behavior. To estimate the window where the zero-momentum mode is important, we estimate the two modes' relative contribution to the effective conductivity. We find [61]

$$\frac{\sigma_z}{\sigma_F} \sim \frac{(k_B T)^2}{\mu^2}\left[\frac{l_{ee}^2}{L^2} + \frac{\gamma_{imp}}{\gamma_{ee}}\right], \tag{17}$$

where σ_z and σ_F correspond to the zero-momentum and finite-momentum (hydrodynamic) conductivities, respectively, and L is the sample length. Therefore, even in the Dirac fluid limit, the zero-momentum mode can be neglected so long as $\mu^2/(k_B T)^2 \gg l_{ee}^2/L^2 + \gamma_{imp}/\gamma_{ee}$, where the rhs is small in the hydrodynamic limit. Where this inequality is satisfied, our main result, Eq. (10), applies directly; where it is violated, the Ohmic result Eq. (3) applies. We remark that one can make more rigorous estimates using the explicit expressions from Boltzmann kinetic theory [26,41,65] which give the same functional form.

While for a rectangular geometry the geometric correction f to the Johnson noise does not deviate greatly from unity, one may wonder whether this conclusion is strongly geometry dependent. More specifically, one can ask about the annular Corbino geometry; it exhibits "paradoxical" behavior for hydrodynamic electron flow, with a near-vanishing of the bulk electric field even when a strong current is flowing [38–40,66,67]. If one naïvely applies the Shockley-Ramo theorem [68–71], then this bulk electric field expulsion would seemingly imply that the Johnson noise is unmodified by current flow, even as this flow produces significant electron heating. However, the version of Shockley-Ramo appropriate for an electron fluid [71] relies on a well-defined local conductivity. We expect that the current noise for the Corbino geometry is qualitatively similar to the rectangle; we do not expect any zeros or anomalies, only a quantitative change in the geometric correction. In the Ohmic limit (i.e., small λ), we expect a return to Eq. (3). Moreover, when the two annular radii $r_2 - r_1 \equiv \delta \ll r_1$ are very close, the temperature variations are suppressed by $\mathcal{O}(\delta^2/r_1^2)$, so we also expect the current noise to be Ohmic-like in this 1D limit. We leave further exploration of the Corbino and of other geometries to future work.

We thank Philip Kim, Jonah Waissman, Artem Talanov, Zhongying Yan, Alex Levchenko, Gregory Falkovich, Daniel E. Prober, and Justin C. W. Song for discussions. A. H. was partially supported by the Center for Emergent Materials, an NSF-funded MRSEC, under Grant No. DMR-2011876. B. S. was partly supported by NSF Grant No. DMR-2045742.

[1] The usual expression $\langle I^2 \rangle = 4k_B T_0 \Delta f/R$ can be obtained by convolving with the inverse Fourier transform of a rectangular function (band-pass filter) of width Δf (with low and high band edges set appropriately) and setting $t - t' = 0$. Since we are working with two-sided Fourier transforms, the negative frequencies will provide the additional factor of 2.

[2] B. S. Karasik, C. B. McKitterick, and D. E. Prober, Prospective performance of graphene HEB for ultrasensitive detection of Sub-mm radiation, J. Low Temp. Phys. **176**, 249 (2014).

[3] D. K. Efetov, R.-J. Shiue, Y. Gao, B. Skinner, E. D. Walsh, H. Choi, J. Zheng, C. Tan, G. Grosso, C. Peng, J. Hone, K. C. Fong, and D. Englund, Fast thermal relaxation in cavity-coupled graphene bolometers with a Johnson noise read-out, Nat. Nanotechnol. **13**, 797 (2018).

[4] W. Miao, H. Gao, Z. Wang, W. Zhang, Y. Ren, K. M. Zhou, S. C. Shi, C. Yu, Z. Z. He, Q. B. Liu, and Z. H. Feng, A graphene-based terahertz hot electron bolometer with Johnson noise readout, J. Low Temp. Phys. **193**, 387 (2018).

[5] C. Liu, L. Du, W. Tang, D. Wei, J. Li, L. Wang, G. Chen, X. Chen, and W. Lu, Towards sensitive terahertz detection via thermoelectric manipulation using graphene transistors, NPG Asia Mater. **10**, 318 (2018).

[6] W. Miao, F. M. Li, Z. Z. He, H. Gao, Z. Wang, W. Zhang, Y. Ren, K. M. Zhou, J. Q. Zhong, S. C. Shi, C. Yu, Q. B. Liu, and Z. H. Feng, Demonstration of a high-sensitivity and wide-dynamic-range terahertz graphene hot-electron bolometer with Johnson noise thermometry, Appl. Phys. Lett. **118**, 013104 (2021).

[7] K. C. Fong and K. C. Schwab, Ultrasensitive and Wide-Bandwidth Thermal Measurements of Graphene at Low Temperatures, Phys. Rev. X **2**, 031006 (2012).

[8] J. Crossno, X. Liu, T. A. Ohki, P. Kim, and K. C. Fong, Development of high frequency and wide bandwidth Johnson noise thermometry, Appl. Phys. Lett. **106**, 023121 (2015).

[9] J. Waissman, L. E. Anderson, A. V. Talanov, Z. Yan, Y. J. Shin, D. H. Najafabadi, M. Rezaee, X. Feng, D. G. Nocera, T. Taniguchi, K. Watanabe, B. Skinner, K. A. Matveev, and P. Kim, Electronic thermal transport measurement in low-dimensional materials with graphene non-local noise thermometry, Nat. Nanotechnol. **17**, 166 (2022).

[10] E. V. Sukhorukov and D. Loss, Noise in multiterminal diffusive conductors: Universality, nonlocality, and exchange effects, Phys. Rev. B **59**, 13054 (1999).

[11] C. Pozderac and B. Skinner, Relation between Johnson noise and heating power in a two-terminal conductor, Phys. Rev. B **104**, L161403 (2021).

[12] D. E. Prober, Superconducting terahertz mixer using a transitionedge microbolometer, Appl. Phys. Lett. **62**, 2119 (1993).
[13] A. Lucas and K. C. Fong, Hydrodynamics of electrons in graphene, J. Phys. Condens. Matter **30**, 053001 (2018).
[14] B. N. Narozhny, Hydrodynamic approach to two-dimensional electron systems, Riv. Nuovo Cimento **45**, 661 (2022).
[15] M. J. M. de Jong and L. W. Molenkamp, Hydrodynamic electron flow in high-mobility wires, Phys. Rev. B **51**, 13389 (1995).
[16] M. Müller, J. Schmalian, and L. Fritz, Graphene: A Nearly Perfect Fluid, Phys. Rev. Lett. **103**, 025301 (2009).
[17] I. Torre, A. Tomadin, A. K. Geim, and M. Polini, Nonlocal transport and the hydrodynamic shear viscosity in graphene, Phys. Rev. B **92**, 165433 (2015).
[18] L. Levitov and G. Falkovich, Electron viscosity, current vortices and negative nonlocal resistance in graphene, Nat. Phys. **12**, 672 (2016).
[19] D. A. Bandurin, I. Torre, R. K. Kumar, M. B. Shalom, A. Tomadin, A. Principi, G. H. Auton, E. Khestanova, K. S. Novoselov, I. V. Grigorieva, L. A. Ponomarenko, A. K. Geim, and M. Polini, Negative local resistance caused by viscous electron backflow in graphene, Science **351**, 1055 (2016).
[20] J. Crossno, J. K. Shi, K. Wang, X. Liu, A. Harzheim, A. Lucas, S. Sachdev, P. Kim, T. Taniguchi, K. Watanabe, T. A. Ohki, and K. C. Fong, Observation of the Dirac fluid and the breakdown of the Wiedemann-Franz law in graphene, Science **351**, 1058 (2016).
[21] H. Guo, E. Ilseven, G. Falkovich, and L. S. Levitov, Higher-than-ballistic conduction of viscous electron flows, Proc. Natl. Acad. Sci. U.S.A. **114**, 3068 (2017).
[22] R. Krishna Kumar, D. A. Bandurin, F. M. D. Pellegrino, Y. Cao, A. Principi, H. Guo, G. H. Auton, M. Ben Shalom, L. A. Ponomarenko, G. Falkovich, K. Watanabe, T. Taniguchi, I. V. Grigorieva, L. S. Levitov, M. Polini, and A. K. Geim, Superballistic flow of viscous electron fluid through graphene constrictions, Nat. Phys. **13**, 1182 (2017).
[23] D. A. Bandurin, A. V. Shytov, L. S. Levitov, R. K. Kumar, A. I. Berdyugin, M. Ben Shalom, I. V. Grigorieva, A. K. Geim, and G. Falkovich, Fluidity onset in graphene, Nat. Commun. **9**, 4533 (2018).
[24] B. A. Braem, F. M. D. Pellegrino, A. Principi, M. Röösli, C. Gold, S. Hennel, J. V. Koski, M. Berl, W. Dietsche, W. Wegscheider, M. Polini, T. Ihn, and K. Ensslin, Scanning gate microscopy in a viscous electron fluid, Phys. Rev. B **98**, 241304(R) (2018).
[25] A. I. Berdyugin, S. G. Xu, F. M. D. Pellegrino, R. K. Kumar, A. Principi, I. Torre, M. B. Shalom, T. Taniguchi, K. Watanabe, I. V. Grigorieva, M. Polini, A. K. Geim, and D. A. Bandurin, Measuring Hall viscosity of graphene's electron fluid, Science **364**, 162 (2019).
[26] P. Gallagher, C.-S. Yang, T. Lyu, F. Tian, R. Kou, H. Zhang, K. Watanabe, T. Taniguchi, and F. Wang, Quantum-critical conductivity of the Dirac fluid in graphene, Science **364**, 158 (2019).
[27] J. A. Sulpizio, L. Ella, A. Rozen, J. Birkbeck, D. J. Perello, D. Dutta, M. Ben-Shalom, T. Taniguchi, K. Watanabe, T. Holder, R. Queiroz, A. Principi, A. Stern, T. Scaffidi, A. K. Geim, and S. Ilani, Visualizing poiseuille flow of hydrodynamic electrons, Nature (London) **576**, 75 (2019).
[28] A. Jenkins, S. Baumann, H. Zhou, S. A. Meynell, D. Yang, K. Watanabe, T. Taniguchi, A. Lucas, A. F. Young, and A. C. B. Jayich, Imaging the breakdown of Ohmic transport in graphene Phys. Rev. Lett. **129**, 087701 (2022).
[29] M. J. H. Ku, T. X. Zhou, Q. Li, Y. J. Shin, J. K. Shi, C. Burch, L. E. Anderson, A. T. Pierce, Y. Xie, A. Hamo, U. Vool, H. Zhang, F. Casola, T. Taniguchi, K. Watanabe, M. M. Fogler, P. Kim, A. Yacoby, and R. L. Walsworth, Imaging viscous flow of the Dirac fluid in graphene, Nature (London) **583**, 537 (2020).
[30] U. Vool, A. Hamo, G. Varnavides, Y. Wang, T. X. Zhou, N. Kumar, Y. Dovzhenko, Z. Qiu, C. A. C. Garcia, A. T. Pierce, J. Gooth, P. Anikeeva, C. Felser, P. Narang, and A. Yacoby, Imaging phonon-mediated hydrodynamic flow in WTe2, Nat. Phys. **17**, 1216 (2021).
[31] A. Aharon-Steinberg, T. Völkl, A. Kaplan, A. K. Pariari, I. Roy, T. Holder, Y. Wolf, A. Y. Meltzer, Y. Myasoedov, M. E. Huber, B. Yan, G. Falkovich, L. S. Levitov, M. Hücker, and E. Zeldov, Direct observation of vortices in an electron fluid, Nature (London) **607**, 74 (2022).
[32] P. J. W. Moll, P. Kushwaha, N. Nandi, B. Schmidt, and A. P. Mackenzie, Evidence for hydrodynamic electron flow in PdCoO2, Science **351**, 1061 (2016).
[33] M. D. Bachmann, A. L. Sharpe, G. Baker, A. W. Barnard, C. Putzke, T. Scaffidi, N. Nandi, P. H. McGuinness, E. Zhakina, M. Moravec, S. Khim, M. König, D. Goldhaber-Gordon, D. A. Bonn, A. P. Mackenzie, and P. J. W. Moll, Directional ballistic transport in the two-dimensional metal PdCoO2, Nat. Phys. **18**, 819 (2022).
[34] J. Gooth, F. Menges, N. Kumar, V. Süb, C. Shekhar, Y. Sun, U. Drechsler, R. Zierold, C. Felser, and B. Gotsmann, Thermal and electrical signatures of a hydrodynamic electron fluid in tungsten diphosphide, Nat. Commun. **9**, 4093 (2018).
[35] G. M. Gusev, A. D. Levin, E. V. Levinson, and A. K. Bakarov, Viscous electron flow in mesoscopic two-dimensional electron gas, AIP Adv. **8**, 025318 (2018).
[36] A. D. Levin, G. M. Gusev, E. V. Levinson, Z. D. Kvon, and A. K. Bakarov, Vorticity-induced negative nonlocal resistance in a viscous two-dimensional electron system, Phys. Rev. B **97**, 245308 (2018).
[37] G. M. Gusev, A. S. Jaroshevich, A. D. Levin, Z. D. Kvon, and A. K. Bakarov, Stokes flow around an obstacle in viscous two-dimensional electron liquid, Sci. Rep. **10**, 7860 (2020).
[38] M. Shavit, A. Shytov, and G. Falkovich, Freely Flowing Currents and Electric Field Expulsion in Viscous Electronics, Phys. Rev. Lett. **123**, 026801 (2019).
[39] A. Stern, T. Scaffidi, O. Reuven, C. Kumar, J. Birkbeck, and S. Ilani, Spread and Erase—How Electron Hydrodynamics can Eliminate the Landauer-Sharvin Resistance, Phys. Rev. Lett. **129**. 157701 (2021).
[40] C. Kumar, J. Birkbeck, J. A. Sulpizio, D. Perello, T. Taniguchi, K. Watanabe, O. Reuven, T. Scaffidi, A. Stern, A. K. Geim, and S. Ilani, Imaging hydrodynamic electrons flowing without Landauer-Sharvin resistance, Nature (London) **609**, 276 (2022).

[41] M. Müller, L. Fritz, and S. Sachdev, Quantum-critical relativistic magnetotransport in graphene, Phys. Rev. B **78**, 115406 (2008).

[42] M. S. Foster and I. L. Aleiner, Slow imbalance relaxation and thermoelectric transport in graphene, Phys. Rev. B **79**, 085415 (2009).

[43] A. Principi and G. Vignale, Violation of the Wiedemann-Franz Law in Hydrodynamic Electron Liquids, Phys. Rev. Lett. **115**, 056603 (2015).

[44] A. Lucas, R. A. Davison, and S. Sachdev, Hydrodynamic theory of thermoelectric transport and negative magnetoresistance in Weyl semimetals, Proc. Natl. Acad. Sci. U.S.A. **113**, 9463 (2016).

[45] A. Lucas and S. Das Sarma, Electronic hydrodynamics and the breakdown of the Wiedemann-Franz and mott laws in interacting metals, Phys. Rev. B **97**, 245128 (2018).

[46] M. Zarenia, T. B. Smith, A. Principi, and G. Vignale, Breakdown of the Wiedemann-Franz law in *ab*-stacked bilayer graphene, Phys. Rev. B **99**, 161407(R) (2019).

[47] M. Zarenia, A. Principi, and G. Vignale, Thermal transport in compensated semimetals: Effect of electron-electron scattering on Lorenz ratio, Phys. Rev. B **102**, 214304 (2020).

[48] R. A. Robinson, L. Min, S. H. Lee, P. Li, Y. Wang, J. Li, and Z. Mao, Large violation of the Wiedemann–Franz law in Heusler, ferromagnetic, Weyl semimetal Co2MnAl, J. Phys. D **54**, 454001 (2021).

[49] S. Ahn and S. Das Sarma, Hydrodynamics, viscous electron fluid, and Wiedeman-Franz law in two-dimensional semiconductors, Phys. Rev. B **106**, L081303 (2022).

[50] S. Li, A. Levchenko, and A. V. Andreev, Hydrodynamic thermoelectric transport in Corbino geometry, Phys. Rev. B **105**, 125302 (2022).

[51] Incompressibility of flow has a *different* meaning than that of the incompressibility of an electronic system. The former means only that $v \ll c$, while the latter is a statement about the thermodynamic compressibility $dn/d\mu$.

[52] L. Landau and E. Lifshitz, *Fluid Mechanics: Landau and Lifshitz: Course of Theoretical Physics* (Elsevier Science, New York, 2013), Vol. 6.

[53] For an unscreened Coloumb potential in 3D, obeying the constitutive relation $\nabla^2\delta\phi = (\delta\rho_e/\epsilon)$, the incompressibility assumption is valid for $v \ll \omega_p L$, where $\omega_p = \sqrt{(ne^2/m\epsilon)}$ is the plasma frequency for n the number density and ϵ the electric permittivity. Similarly, for the unscreened 2D Coloumb potential, where $\omega \sim \sqrt{k}$, one should take c to be the smallest characteristic group velocity, i.e., $c \sim (d\omega/dk)|_{k=1/L}$.

[54] Here we invoke Reynolds numbers only to justify dropping convection terms from the hydrodynamic equations, and not to estimate the conditions for the onset of turbulence, which in general is suppressed by the presence of static disorder (as measured by the momentum-relaxing Reynolds number).

[55] A. Hui, V. Oganesyan, and E.-A. Kim, Beyond Ohm's law: Bernoulli effect and streaming in electron hydrodynamics, Phys. Rev. B **103**, 235152 (2021).

[56] L. Landau, E. Lifshitz, and L. Pitaevskii, *Course of Theoretical Physics: Statistical Physics, Part 2*, edited by E. M. Lifshitz and L. P. Pitaevskii (Pergamon Press Ltd., Elmsford, 1980), Vol. 9.

[57] Since the correlation function is time-reversal even, from the Laplace transform we can obtain the Fourier transform via the replacement $s \to i\omega$ [56].

[58] S. Kogan, *Electronic Noise and Fluctuations in Solids* (Cambridge University Press, Cambridge, England, 1996).

[59] K. E. Nagaev, Influence of electron-electron scattering on shot noise in diffusive contacts, Phys. Rev. B **52**, 4740 (1995).

[60] The dominance of Johnson noise is experimentally evidenced by the linear relationship between heating power and noise power. This could be because hydrodynamic behavior tends to appear at elevated temperatures ($\gtrsim$100 K), but one may also expect electron-electron interactions to suppress shot noise due to strong positional correlations between electrons.

[61] See Supplemental Material http://link.aps.org/supplemental/10.1103/PhysRevLett.130.256301 for mathematical details, which includes Refs. [56,62,63].

[62] C. Conca, F. Murat, and O. Pironneau, The Stokes and Navier-Stokes equations with boundary conditions involving the pressure, Jpn J. Math. New Ser. **20**, 279 (1994).

[63] B. N. Narozhny, Electronic hydrodynamics in graphene, Ann. Phys. (Amsterdam) **411**, 167979 (2019).

[64] Additional contributions due to relativistic hydrodynamics are negligible in the limit $v \ll v_F$, where v_F is the "speed of light." [13].

[65] Z. Sun, D. N. Basov, and M. M. Fogler, Universal linear and nonlinear electrodynamics of a Dirac fluid, Proc. Natl. Acad. Sci. U.S.A. **115**, 3285 (2018).

[66] A. Hui and B. Skinner, The Corbino paradox for hydrodynamic electrons, J. Club Condens. Matter Phys. (2022), 10.36471/JCCM.

[67] A. Levchenko, S. Li, and A. V. Andreev, Hydrodynamic magnetoresistance in graphene Corbino devices, Phys. Rev. B **106**, L201306 (2022).

[68] W. Shockley, Currents to conductors induced by a moving point charge, J. Appl. Phys. **9**, 635 (1938).

[69] S. Ramo, Currents induced by electron motion, Proc. IRE **27**, 584 (1939).

[70] Z. He, Review of the Shockley–Ramo theorem and its application in semiconductor gamma-ray detectors, Nucl. Instrum. Methods Phys. Res., Sect. A **463**, 250 (2001).

[71] J. C. W. Song and L. S. Levitov, Shockley-Ramo theorem and long-range photocurrent response in gapless materials, Phys. Rev. B **90**, 075415 (2014).